Evidence for modulation of EEG microstate sequence by vigilance level

Marina Krylova [a,b], Sarah Alizadeh [a], Igor Izyurov [b,a], Vanessa Teckentrup [a], Catie Chang [c], Johan van der Meer [f], Michael Erb [g], Nils Kroemer [a], Thomas Koenig [i], Martin Walter [b,a,d,e,h,*], Hamidreza Jamalabadi [a,**]

[a] *Department of Psychiatry and Psychotherapy, Division for Translational Psychiatry, University of Tübingen, Tübingen, Germany*
[b] *Department of Psychiatry and Psychotherapy, Jena University Hospital, Philosophenweg 3, 07743 Jena, Germany*
[c] *Department of Electrical Engineering and Computer Science, Vanderbilt University, Nashville, USA*
[d] *Clinical Affective Neuroimaging Laboratory, Magdeburg, Germany*
[e] *Leibniz Institute for Neurobiology, Magdeburg, Germany*
[f] *QIMR Berghofer Medial Research Institute, Brisbane, Australia*
[g] *Division of Biomedical Magnetic Resonance, University of Tübingen, Tübingen, Germany*
[h] *Max Planck Institute for biological cybernetics, Tübingen, Germany*
[i] *Translational Research Center, University Hospital of Psychiatry and Psychotherapy, University of Bern, Switzerland*

ARTICLE INFO

ABSTRACT

The momentary global functional state of the brain is reflected in its electric field configuration and cluster analytical approaches have consistently shown four configurations, referred to as EEG microstate classes A to D. Changes in microstate parameters are associated with a number of neuropsychiatric disorders, task performance, and mental state establishing their relevance for cognition. However, the common practice to use eye-closed resting state data to assess the temporal dynamics of microstate parameters might induce systematic confounds related to vigilance levels. Here, we studied the dynamics of microstate parameters in two independent data sets and showed that the parameters of microstates are strongly associated with vigilance level assessed both by EEG power analysis and fMRI global signal. We found that the duration and contribution of microstate class C, as well as transition probabilities towards microstate class C were positively associated with vigilance, whereas the sign was reversed for microstate classes A and B. Furthermore, in looking for the origins of the correspondence between microstates and vigilance level, we found Granger-causal effects of vigilance levels on microstate sequence parameters. Collectively, our findings suggest that duration and occurrence of microstates have a different origin and possibly reflect different physiological processes. Finally, our findings indicate the need for taking vigilance levels into consideration in resting-sate EEG investigations.

1. Introduction

The topographical distribution of brain electrical potentials reflects the large-scale brain activity which can be effectively measured using multichannel scalp EEG (Fallgatter et al., 1997, Fallgatter et al., 2001, Hallez et al., 2007, Lehmann & Skrandies, 1984). Intriguingly, these topographical configurations do not change randomly but remain quasi-stable for a short period of time of around 80 milliseconds before rapidly switching to another quasi-stable topography. These reoccurring stable geometrical patterns are referred to as EEG microstates (Lehmann et al., 1987). Clustering approaches have consistently revealed four prototypical topographies which are sufficient to explain around 80% of variance in resting-state recordings (Khanna et al., 2014, Khanna et al., 2015,

Koenig et al., 2002, Michel & Koenig, 2017), where the polarity can invert reflecting oscillations of the dominant generators.

As expected, the temporal characteristics of EEG microstate sequences change in response to a large number of external and internal stimulations. These include but are not limited to content of spontaneous thoughts (Lehmann et al., 2010), behavioral (Dimitriadis et al., 2015, Milz et al., 2016, Seitzman et al., 2017) and global brain state (Faber et al., 2005, Katayama et al., 2007) as well as pharmacological manipulations (Schiller et al., 2019). These characteristics are different in patients suffering from neuropsychiatric disorders, such as schizophrenia, depression, dementia and multiple others (for a review see Khanna et al., 2015, Michel & Koenig, 2017).

An important but often neglected aspect of these works, however, is that most of these studies were conducted using eyes-closed resting

state EEG recordings alone. During typical eyes-closed rest, subjects tend to sequentially transit from complete wakefulness towards drowsiness. Tagliazucchi and Lafus in 2014 showed that likelihood of subjects falling asleep during eyes-closed recordings is high, and approximately half of the participants loose wakefulness after 10 minutes (Tagliazucchi & Laufs, 2014). While the probability of subjects falling sleep varies depending on the experimental conditions (Tagliazucchi & Laufs, 2014), majority of subjects experience drowsiness, an intermediate state between wakefulness and sleep onset (Mathis & Hess, 2009) characterized by slowed reactions and reduced attention (Cori et al., 2019). Transition from complete wakefulness to sleep onset is characterized by strong occipital alpha power increase immediately after closing the eyes that is followed up by anteriorization of alpha power focus (De Gennaro et al., 2005) and subsequent increase of delta and theta activity indicating further transition to drowsiness (Olbrich et al., 2009, Strijkstra et al., 2003).

As classification of EEG microstate classes is strongly dependent on the power of alpha frequency (Lehmann et al., 1987), it is reasonable to hypothesize that the temporal characteristics of EEG microstates might be affected by vigilance changes. Since patients suffering from neuropsychiatric disorders are known to have altered vigilance regulation pattern (Hegerl & Hensch, 2014, Olbrich et al., 2012, Strauss et al., 2015), this hypothesis, should it get confirmed, can have strong implications in interpreting EEG microstate alterations in a clinical context (for a related topic see Zanesco et al., 2020).

To test this hypothesis, we investigated the relation of the characteristics of EEG microstate parameters with vigilance levels using two independent data sets of simultaneous eyes-closed EEG/fMRI resting state recordings. These datasets allowed us to 1) test the association of EEG microstate parameters with vigilance estimates based on EEG as well as fMRI metrics, and 2) assess potential causal relationship between vigilance loss and changes in temporal dynamics of EEG microstate characteristics.

2. Methods

2.1. Data Acquisition

The analysis was performed on two independent data sets of simultaneous EEG/fMRI recordings. The first study is registered at ClinicalTrials.gov, number NCT02602275 (date of registration: 28/10/2015) and approved by the ethics committee of the University of Magdeburg as well as the Competent Authority (Federal Institute for Drugs and Medical Devices). The second study was approved by the Ethics Committee of the University of Tübingen, Germany. A written informed consent was signed by each participant prior to any study participation.

2.1.1. Data set 1

The first data set includes 12-min eyes-closed resting-state recordings of 39 healthy male volunteers (mean age 43.7 ± 9.8) over one session of simultaneous EEG and 3-Tesla fMRI. EEG data were acquired using the BrainAmp MR system (Brain Products) with a 64-channel EasyCap. One channel placed on the back was used for ECG detection. AFz was used as reference electrode and FCz as ground electrode. The sampling rate was 5000 Hz. To increase the quality of EEG in simultaneous EEG-fMRI recordings, EEG cap was augmented with six carbon wire loops (CWLs) (van der Meer et al., 2016). Four CWLs were placed on the outer surface of the EEG cap at the left and right frontal and left and right posterior locations, and two CWLs were attached to the cables connecting the EEG cap to the EEG amplifier (BrainAmpMR Plus). Imaging data were acquired on a 3 Tesla Philips whole body MRI system (Philips Medical Systems, Hamburg, Germany). First, structural T1-weighted images for spatial normalization were measured using a turbo field echo (TFE) sequence (274 sagittal slices covering the whole brain, flip angle = 8°, 256 × 256 matrix, voxel size = 2.5 × 2.5 × 3 mm^3). Whole brain BOLD resting-state data were acquired over 34 axial slices using an echo planar imaging (Randerath et al.,) sequence (TR = 2,000 ms,

TE = 30 ms, flip angle = 90°, 96 × 94 matrix, field of view = 24 cm, voxel size = 2.5 × 2.5 × 3 mm^3).

2.1.2. Data set 2

The second data set includes 10-min eyes-closed resting-state recordings of 20 healthy male volunteers (mean age 26.8 ± 7.6) over one session of simultaneous EEG and 3-Tesla fMRI. EEG data were acquired with the same parameters as in data set 1. Imaging data were acquired on a 3 Tesla Siemens Prisma whole body MRI system (Siemens Medical Solutions, Erlangen, Germany). First, structural T1-weighted images for spatial normalization were measured using a three-dimensional magnetization-prepared rapid gradient echo (MP-RAGE) sequence (192 sagittal slices covering the whole brain, flip angle = 9°, 256 × 256 matrix, voxel size = 1 × 1 × 1 mm^3, PE-GRAPPA factor 2). Whole brain BOLD resting-state data were acquired over 30 axial slices using an echo planar imaging (Randerath et al., 2017) sequence (TR = 1,800 ms, TE = 35 ms, flip angle = 79°, 64 × 64 matrix, field of view = 19.2 cm, voxel size = 3 × 3 × 4 mm^3).

2.2. Data Preprocessing

2.2.1. Electroencephalography

First, gradient artifacts were removed from the EEG data by a motion informed template subtraction realized by the Bergen EEG-fMRI toolbox (Moosmann et al., 2009) using a MRI template waveform obtained from 25 MRI artifacts in a sliding window manner (Allen et al., 2000). Next, EEG data was first bandpass filtered between 0.3Hz to 200Hz and down-sampled to 1000Hz. The helium pump and ballistocardiac (BCG) artifacts were then removed using the Carbon-wire loop technique (van der Meer et al., 2016). Next, the data were segmented into 2s and 1.8s epochs for the data set 1 and 2 respectively (i.e. equivalent to the TR of the BOLD resting-state scans), and the epochs containing muscle and head movement artifacts (outliers in spectral power between 110 and 140 Hz) were removed. The channels that contained more than 50% of epochs with artifacts were interpolated using routines provided by EEGLAB (Delorme & Makeig, 2004). Finally, ICA decomposition of the EEG data was performed and components reflecting eye movements, continuous muscle activity and residual MRI-artefacts were removed. Six subjects from data set 1 and one subject from data set 2 were excluded from further analysis because of their low EEG quality or technical problems during data acquisition.

2.2.2. Functional MRI

fMRI data were preprocessed using SPM12 (FIL, Wellcome Trust Centre for Human Neuroimaging, UCL, London, UK) toolbox. The first three volumes of each recording were excluded from the analysis. The functional corrections included slice time correction and realignment to the first image. The structural T1-weighted volume was registered to the mean functional image and segmented, in order to normalize functional and structural images to the Montreal Neurological Institute (MNI) template brain. Normalized functional volumes were then smoothed with a three-dimensional Gaussian kernel of 6 mm full-width-half-maximum. Finally, each voxel time-course was normalized by subtracting the mean value and dividing the resulting difference to the mean value. Global signal time course was then estimated by averaging the normalized time-series across all voxels with a gray matter tissue probability of at least 60% (based on tissue probability maps from the SPM12 toolbox). The global signal time-series were smoothed by calculating the mean values within a non-overlapping window of 3 TR.

2.2.3. Microstate extraction

EEG microstate (MS) analysis was performed separately for each dataset using the EEGLAB plugin for Microstates version 1.1, developed
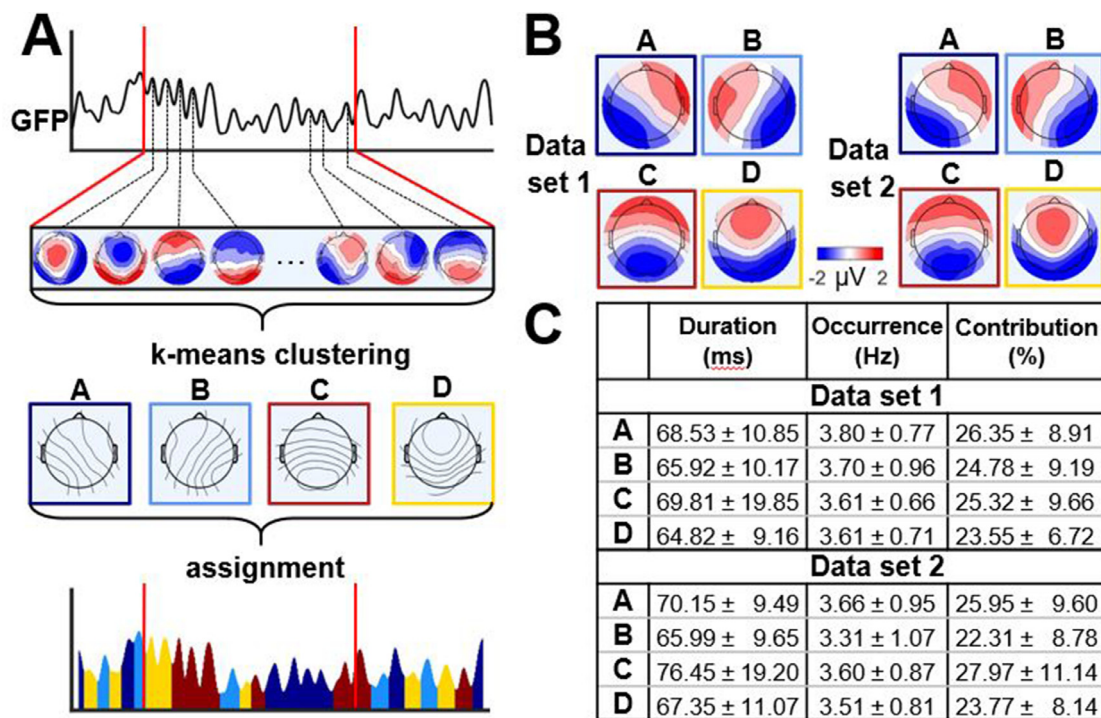
Fig. 1. Microstate extraction and the parameters (A) Schematic representation of the microstate extraction procedure: 1) Global Field Power (GFP) is calculated at each time point of the multichannel EEG recording. 2) The head-surface potential maps at the peaks of the GFP curve are extracted and submitted to the clustering algorithm to reveal the dominant topographies (EEG microstates). 3) The original maps at peaks of the GFP curve are assigned to one of the microstate classes A, B, C, or D based on the degree of the spatial similarity with the microstate maps. (B) Head-surface topographies of the four EEG microstate classes for data set 1 (on the left) and data set 2 (on the right) during eyes closed resting. C: The microstate parameters for the four microstate classes (mean ± standard deviation).

by Thomas König (http://www.thomaskoenig.ch/index.php/software/microstates-in-eeglab). Artefact-free EEG data were re-referenced to average reference, bandpass filtered between 2 and 20 Hz and further down-sampled to 250 Hz. The Global Field Power (GFP) was calculated as the root of the mean of the squared potential differences at all electrodes from the mean of instantaneous potentials across electrodes. Since the topography remains stable around peaks of the GFP, they are the best representative of the momentary map topography in terms of signal to-noise ratio (Koenig et al., 2005). All maps marked as GFP peaks were extracted and submitted to a modified k-means clustering algorithm to deduce four classes of map topographies (microstates) that maximally explain the variance of the GFP peak map topographies. These four classes of map topographies were then submitted to a full permutation procedure (Koenig et al., 1999) to compute mean classes across participants. Using the mean microstate classes across subjects as templates, for all participants the EEG topographies at the moments of GFP peaks were assigned to one of these four microstates based on maximal absolute value of Pearson correlation. Successive GFP peak maps assigned to the same class were recognized as belonging to one microstate. Time points between GFP peaks were assigned to the microstate class of the temporally closest GFP peak (Fig. 1A). In each epoch the time points before the first and after the last detected GFP peak were excluded because microstates cannot be determined in these points. For each microstate class and each epoch, four parameters were estimated i.e. duration (i.e. mean time spent in the current MS class), occurrence (i.e. frequency of appearance of the current MS class), contribution (i.e. percentage of total time of recording spent in the current MS class), and transition probability. As the observed transition probability might be affected by differences in occurrence between microstate classes, we also estimated a random transition probability model as described by Lehmann et al. (Lehmann et al., 2005). The resulting transition probability was calculated as the difference between the observed transition probability and the one estimated from the random transition probability model. To get rid of the fast fluctuations, the time course of the microstate parameters was smoothed by calculating the mean value within a non-overlapping window of 3 TR (resulting in 6 s and 5.6 s window length for dataset 1 and 2 respectively).

2.3. Estimation of vigilance level

As the EEG recordings did not contain electrooculography data, the use of conventional vigilance calculation algorithm (VIGALL; Vigilance Algorithm Leipzig) (Olbrich et al., 2009) was not suitable for these data. To obtain the temporal dynamics of vigilance fluctuation, power spectral density of EEG was estimated for each channel using non-overlapping Hamming window (data set 1: 500 points, 2.0s temporal width. data set 2: 450 points, 1.8s temporal width). The temporal resolution of the spectrogram was equivalent to the TR of fMRI resting state scans (i.e. 2s and 1.8s for the data set 1 and 2 respectively). Next, we estimated the global spectrogram by computing the root mean square (rms) value across all channels at each frequency. Then, vigilance time-series were calculated as rms amplitude in the alpha frequency band (7-13 Hz) divided by the rms amplitudes in the delta and theta frequency band (1-7 Hz) at each time point. The similar approach was used by (Falahpour et al., 2018). To evaluate the reliability of the vigilance measure, vigilance scores for data set 1 were extracted using VIGALL 2.1 (Hegerl et al., 2017) and a correlation analysis comparing the outputs of the two approaches was performed (for details see Appendix A). Additionally, the individual EEG data were visually inspected for the indicators of the early sleep stage (sleep spindles and K-complexes) that were present in the EEG of only two subjects (two K-complexes in one subject and several instances of K-complexes in the window from 5.2 – 7.6 min of the recording) in data set 1. Due to rare occurrence of these events, these subjects were not excluded from the further analysis. To omit the fast fluctuations, the vigilance time-series were smoothed by calculating the mean value within a non-overlapping window of 3 TR.

2.4. Statistical analysis

2.4.1. Assessment of the association between vigilance level, microstate parameters, and the global signal

We analyzed the association between microstate parameters and vigilance on two levels. First, accounting for the between subject variability (Tagliazucchi & Laufs, 2014), we estimated the association between vigilance level and microstate parameters in terms of the Pearson correlation between mean vigilance and mean values of microstate parameters across subjects. To account for multiple testing, results were adjusted using False Discovery Rate (FDR) correction over 12 comparisons (for details see Section 1.4.2).

Second, we inspected the temporal correlations between microstate parameters and vigilance level. For each subject, the Pearson correlation between the vigilance time-series and the time courses of each one of the microstate parameters were calculated. To account for the potential inflation of the Pearson correlation coefficients caused by long-term autocorrelation present in EEG data (Allefeld et al., 2008), we corrected the tests using a novel correction approach (Afyouni et al., 2019). xDF accounts for distinct autocorrelation in each time series for instantaneous and lagged cross-correlation. We used one-sample t-tests on the xDF-adjusted z-scored correlation coefficients to estimate the group level effects. Results were corrected using FDR correction over 12 comparisons (for details see Section 1.4.2). To investigate frequency dependence of the microstate parameters, we repeated the analysis of the EEG frequency power in alpha and delta+theta frequency ranges and microstate parameters (for details see Appendix B).

To investigate the association of the temporal dynamics of the microstate parameters with the global signal, vigilance and microstate parameters' time-series were convolved with the canonical hemodynamic response function of SPM12 toolbox (FIL, Wellcome Trust Centre for Human Neuroimaging, UCL, London, UK) to account for the hemodynamic delay. For each subject the linear Pearson correlation between the vigilance time-series and the time course of the fMRI global signal as well as the linear Pearson correlation between each microstate parameter and the time course of the fMRI global signal were calculated. We used one-sample t-tests on the xDF-adjusted z-scored correlation coefficients to estimate the group level association. Results were adjusted using FDR correction over 12 comparisons (for details see section 1.4.2).

2.4.2. Multiple comparisons

The EEG microstate parameters are strongly interrelated (i.e. higher occurrence and longer duration lead to higher contribution of the microstate and higher occurrence is linked to increased transition probabilities). However, the dependence of the transition probabilities and occurrence was already accounted for, as the transition probabilities are estimated as the difference between the observed and the estimated from the random transition probability model (Lehmann et al., 2005) ones (see Microstate extraction section for details). Therefore, results were adjusted using False Discovery Rate (FDR) correction over 12 comparisons (either 4 microstate classes x 3 parameters (duration, occurrence, and contribution) or 12 transition probabilities).

2.4.3. Multivariate pattern classification

To test if the univariate correlations observed in previous correlation analysis allow for a temporal reconstruction of the vigilance level, we used support vector machine regression to predict the vigilance time-series based on the parameters of microstates. The prediction was based on twenty-four parameters of microstates (4xDuration, 4xOccurrence, 4xContribution, 12 Transition probabilities). To account for the between-subject variability, the values of each microstate parameter were normalized between 0 and 1 by subtracting the minimum and dividing to the difference between maximal and minimal values of parameter for the whole time-course of the subject. The classification was done using support vector machine regression implemented in MATLAB

function fitrsvm, linear kernel, box constraint of 1 and Karush-Kuhn-Tucker (KKT) violation tolerance of 0.001. We used subject level 2-fold cross-validation, that is, half of the subjects was used for training and the other nonoverlapping half were used to test the model. The whole procedure was repeated 100 times where the subjects were randomly assigned to the train and test sets. Performance of the model was estimated in terms of Pearson correlation between estimated and measured vigilance time-series. To test against the null distribution, we randomly swapped the microstate parameter time courses across different subjects and repeated the prediction procedure 1000 times. Finally, we tested if the effects can be transferred across data sets. To do this, we used support vector machine regression with the same settings. We trained the model on the data of all subjects from the first data set and tested on the data of all subjects from the second data set and vice versa. To test against the null distribution, we randomly swapped the microstate parameter time courses across different subjects within a training data set and repeated the prediction procedure 1000 times.

2.4.4. Causal effects assessment

To test for potential causal effects between microstate parameters and vigilance fluctuations, we calculated Granger causality (GC) which is a well-established measure of lag-based predictive causality. To this end, we used the MVGC toolbox (Barnett & Seth, 2014) where we calculated GC between time courses of the microstate parameters and vigilance time-series. For each participant within the two datasets, for each microstate class and each microstate parameter, we first estimated the optimal lag based on the Bayesian information criterion (BIC). Since for most of the subjects the optimal model order (lag steps) was 1 (89.2% and 87.7% for the data set 1 and 2 respectively), we used this value for all other subjects. We then calculated time-domain pairwise-conditional GC values with a model order of 1 using the source and target pairs microstate parameter/vigilance. To estimate directionality, we obtained delta GC values, contrasting direction and modality. Hence, to estimate the extent to which the vigilance time-series (Vig) Granger-causes the duration-based time-series of microstate A (MSAduration), GC values for the direction MSAduration → Vig were subtracted from GC values for the direction Vig → MSAduration resulting in a delta GC value. For statistical analyses, we bootstrapped the distribution of the mean delta GC values across all subjects with 50000 repetitions using bootci in Matlab2018a. We then calculated p_{boot}-values by summing cases for which the bootstrapped mean delta GC value, depending on the direction of the effect, exceeded or went below zero and divided the sum by the number of iterations. Thus, positive delta GC value would indicate causal effects of vigilance on the microstate parameter, while negative would indicate modulation in opposite direction. Finally, to obtain two-tailed p_{boot}-values we multiplied these values by two.

3. Results

3.1. EEG microstates

Four EEG microstate classes (Fig. 1B) explained on average 77.8 ± 2.9% and 76. 1 ± 3.6% of the total topographic variance across participants for data sets 1 and 2 respectively. Fig. 1C shows mean duration, mean occurrence, and mean contribution for two data sets. The parameters of microstates are well in line with ranges reported in the literature (Khanna et al., 2015, Kikuchi et al., 2011, Kindler et al., 2011, Milz et al., 2016).

3.2. Correlation between vigilance level and microstate parameters

Pearson correlation between mean vigilance levels and mean values of microstate parameters (Fig. 2) revealed significant positive association of the mean vigilance level with mean duration and contribution of microstate class C in both investigated data sets. Mean occurrence of microstate class B was negatively correlated with vigilance levels in
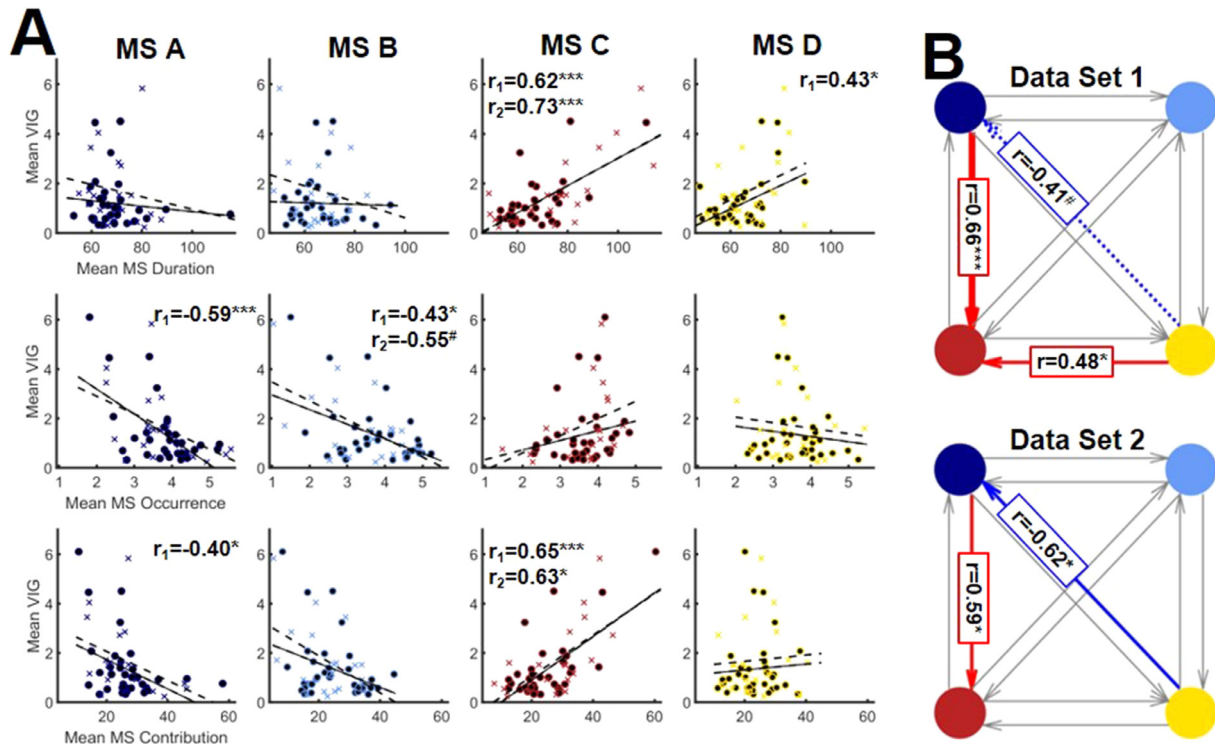
Fig. 2. Association of the mean vigilance level and mean values of the EEG microstate parameters of the four microstate classes during eyes closed resting for the two data sets. A: Top panel: duration, middle panel: occurrence, bottom panel: contribution. Each dot represents data of one subject. Data for the first dataset are presented in circles and solid lines, data for the second dataset are presented in crosses and dashed lines. Mean duration and contribution of the microstate class C were positively, while occurrence of the microstates class B was negatively associated with vigilance level in both investigated datasets. Also, for the first dataset we observe negative association of the occurrence of the microstate class A with vigilance. B: The transition probabilities of the transitions between the four microstate classes. Red arrows represent positive association with vigilance level, blue – negative. The thickness of the line and the number of the stars corresponds to the p-value ($p < 0.001$ – thick / ***, $0.001 < p < 0.01$ – medium / **, $0.01 < p < 0.05$ – thin / *, trend level ($p < 0.065$) – dashed / #) after FDR correction for 12 comparisons. For both data sets mean transition probabilities towards microstate class C were positively, while transition probabilities from microstate class D towards microstate class A were negatively associated with vigilance levels.

the first data set and showed a considerable trend toward significance ($p = 0.058$) in the second data set. Also, occurrence and contribution of the microstate class A showed negative, while duration of microstate class D showed positive association with mean vigilance level with (see Appendix Table C1 for details). Consistent with these findings, we found a significant positive association of probability of transitions towards microstate class C from microstate class A (see Appendix Table C2 for details) and a significant trend towards a negative association of probability of transitions from microstate class D towards microstate class A (data set 1: $p = 0.0638$ data set 2: $p = 0.0499$) with vigilance levels. Interestingly, the higher vigilance level was characterized by increased duration of the microstate class C and decreased occurrence of the microstate class B. Also, the pathway of the transitions between different microstate classes was altered together with changes in vigilance level, with higher probability for transitions towards microstate class C.

In line with the findings in the previous section, temporal correlation between vigilance time-series and the time courses showed significant positive association of the time courses of the duration and contribution of the microstate class C with vigilance. The time courses of the occurrence and contribution of the microstate classes A and B were negatively associated with vigilance (Fig. 3 A). However, we also observed, that the time course of the duration of the microstate class D was positively associated with vigilance time-series (see Appendix Table D1 for details). Also, we observed a positive correlation between the vigilance time course and the time courses of the transition probability for the transitions from the microstate class A towards microstate class C (data set 1: $p < 0.001$, data set 2: $p = 0.064$). The other associations did not

show consistent results for the two data sets (see Appendix Table D2 for details).

3.3. Multivariate pattern classification of the full vigilance time-series based on the microstate parameters

The temporal reconstruction of the vigilance level based on the parameters of the EEG microstates using support vector machine regression showed that both within- and between-dataset predictions are possible (Fig. 4). For both data sets, correlation between estimated and measured vigilance time-series were significantly above chance level ($p < 0.001$). Notably the test and train accuracies for cross dataset tests are quite comparable (Train data set 1, Test data set 2: $r_{train} = 0.66$, $r_{test} = 0.51$; Train data set 2, Test data set 1: $r_{train} = 0.57$, $r_{test} = 0.63$) which speaks for the successful transfer of vigilance metrics across two datasets while the exact r-values are potentially affected by different sample size of two data sets.

3.4. Correlation between time course of microstate parameters and BOLD global signal

We found significant negative correlation between the time course of vigilance levels and the time course of the global signal for both datasets (data set 1: $t = -6.21$, $p < 6 \times 10^{-7}$, data set 2: $t = -4.35$, $p = 4 \times 10^{-4}$). The time courses of the duration and contribution of the microstate class C were negatively (data set 1: $p = 0.014$, data set 2: $p = 0.046$) correlated with global signal and the time course of contribution of mi-
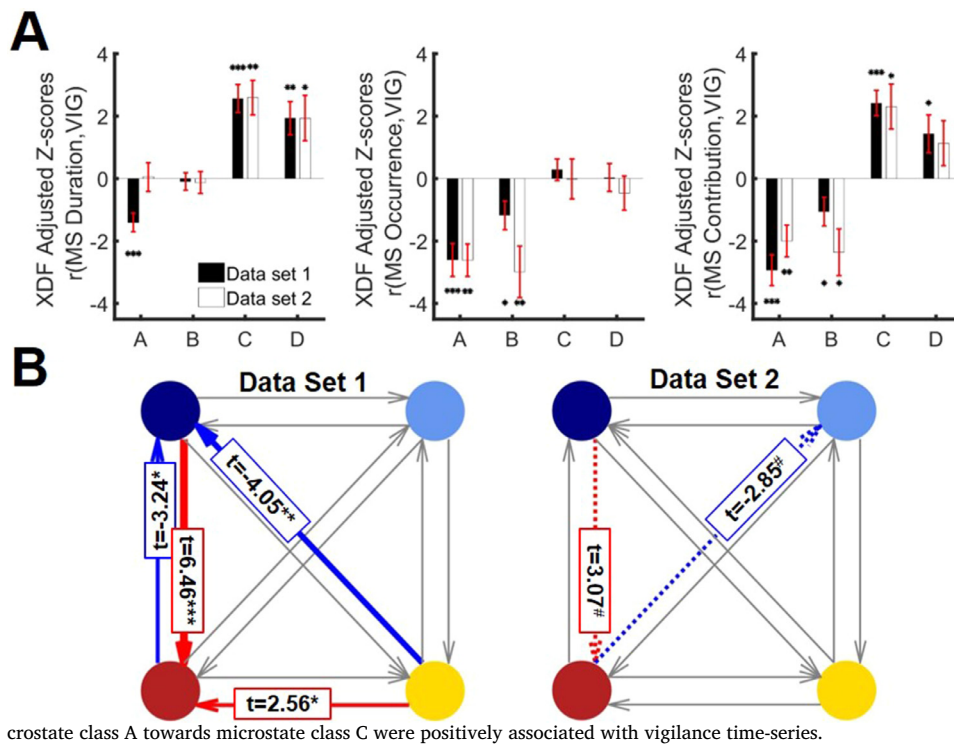
Fig. 3. Association between the vigilance time-series and the time courses of the EEG microstate parameters during eyes closed resting for the two data sets. A: Top panel: duration, middle panel: occurrence, bottom panel: contribution. Bars show group average xDF adjusted Z-scored correlation coefficients for the first (black) and second dataset (white), error bars represent standard deviation of the mean. Stars correspond to the significance levels after FDR correction for 12 comparisons ($p < 0.001$ - ***, $0.001 < p < 0.01$ – **, $0.01 < p < 0.05$ – *). Time courses of the duration and contribution of the microstate class C as well as duration of the microstate class D were positively, while time courses of the occurrence and contribution of the microstates class A and B were negatively associated with change of vigilance level in both investigated data sets. B: The transition probabilities of the transitions between the four microstate classes. Red arrows represent positive association, blue – negative. The thickness of the line corresponds to the p-value ($p < 0.001$ – thick, $0.001 < p < 0.01$ – medium, $0.01 < p < 0.05$ – thin, trend level ($p < 0.065$) - dashed) after FDR correction for 12 comparisons. For both data sets time courses of the transition probabilities for transitions from microstate class A towards microstate class C were positively associated with vigilance time-series.
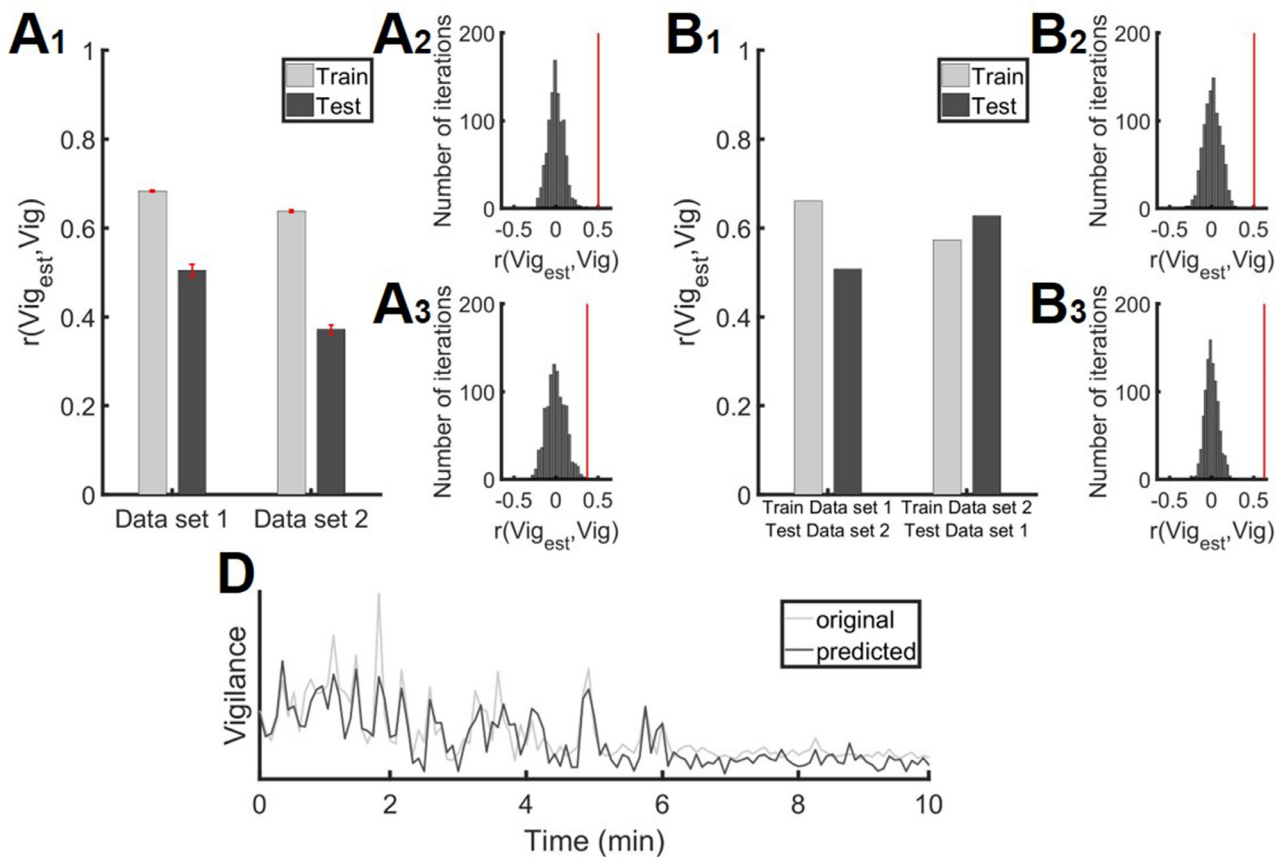

Fig. 4. Prediction of the vigilance time-series based on the EEG microstate parameters using Support Vector Regression (SVR). A: results for a within dataset prediction. A1: correlation between estimated and real vigilance time-series for train (light gray) and test (dark gray). Error bars represent the standard deviation of the mean over 100 repetitions of the train and test procedure. A2,A3: null distribution for the first (A2) and second (A3) dataset. Vertical red line represents the mean test correlation between estimated and real vigilance time-series. B: results for a between dataset prediction. B1: correlation between estimated and real vigilance time-series for train (light gray) and test (dark gray). B2,B3: null distribution for the training on the first dataset and testing on the second dataset (B2) and vice versa (B3). Vertical red line represents the mean test correlation between estimated and real vigilance time-series. D: example of the vigilance time-series prediction for a 10 min interval. Original data are shown in light gray and predicted in dark gray.
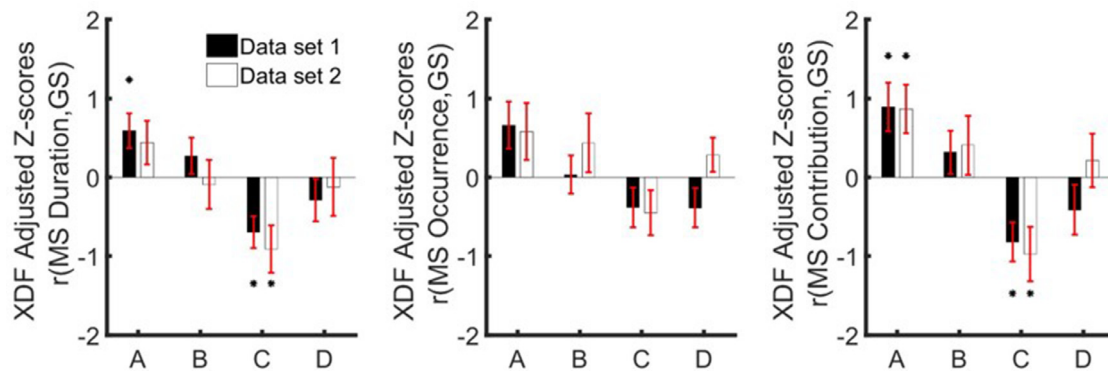
Fig. 5. Association between the fMRI global signal time-series and the time course of the EEG microstate parameters during eyes closed resting for the two datasets. The right panel: duration, middle panel: occurrence, bottom panel: contribution. Bars show group average xDF adjusted Z-scored correlation coefficients for the first (black) and second dataset (white), error bars represent standard deviation of the mean. Stars correspond to the significance levels (p < 0.001 - ***, 0.001 < p < 0.01 – **, 0.01 < p < 0.05 – *) after FDR correction for 12 comparisons. Time courses of the duration and contribution of the microstate class C were negatively, while time courses of the duration and contribution of the microstate class A were positively associated with time course of global signal in both datasets.

Table 1

This table lists the results (95% bootstrap confidence interval and two-tailed p_{boot}-values of the bootstrapped statistics) of the causal relationships between time courses of the microstate parameters and vigilance time-series. Significant results ($p_{boot} < 0.05$) are marked in bold.

	Duration (ms) Confidence interval		p_{boot}	Occurrence (Hz) Confidence interval		p_{boot}	Contribution (%) Confidence interval		p_{boot}
Data set 1									
(Vig → A) – (A → Vig)	-0.022	-0.004	**0.003****	-0.036	-0.011	**0.001*****	-0.036	-0.012	**0.001*****
(Vig → B) – (B → Vig)	-0.019	-0.001	0.057	-0.020	-0.001	**0.033***	-0.022	-0.002	**0.017***
(Vig → C) – (C → Vig)	-0.026	-0.004	**0.006****	-0.019	0.010	0.630	-0.019	0.007	0.422
(Vig → D) – (D → Vig)	-0.028	-0.003	**0.018***	-0.020	-0.001	**0.037***	-0.012	0.008	0.886
Data set 2									
(Vig → A) – (A → Vig)	-0.035	-0.002	**0.048***	-0.068	-0.021	**0.001*****	-0.064	-0.017	**0.001*****
(Vig → B) – (B → Vig)	-0.016	0.018	1	-0.039	-0.014	**0.001*****	-0.034	0.006	0.263
(Vig → C) – (C → Vig)	-0.036	-0.005	**0.008****	-0.017	0.001	0.083	-0.021	0.005	0.316
(Vig → D) – (D → Vig)	-0.040	-0.012	**0.001*****	-0.017	0.003	0.194	-0.023	0.004	0.130

Stars correspond to the significance levels ($p_{boot} < 0.001$ - ***, $0.001 < p_{boot} < 0.01$ – **, $0.01 < p_{boot} < 0.05$ – *). Changes in vigilance levels had causal effect on the changes of the parameters of microstates.

crostate class A was positively correlated (data set 1: p = 0.027, data set 2: p = 0.046) with global signal (Fig. 5). Interestingly, parameters of microstate class B did not show associations with the global signal (see Appendix Table E1 for details). Along the same line, associations between the global signal time course and the time course of transition probabilities of microstates were weak and did not reach significance.

3.5. Causal effects of vigilance on microstate parameters

Granger causality (GC) estimates of the temporal dynamics of the interplay between microstate parameters and vigilance fluctuations revealed causal effect of changes in vigilance on the temporal characteristics of microstate parameters with a model order (lag steps) of 1. For both data sets, changes in vigilance Granger-caused changes in the duration, occurrence and contribution of microstate class A, occurrence of microstate class B and duration of microstate classes C and D (for details see Table 1 and Fig. F.1).

4. Discussion

The temporal dynamics of microstates has been shown to reflect many cognitive processes and to be associated with a large number of psychiatric disorders. Here, looking into two independent datasets, we found that the temporal structure of microstates covaries with the vigilance level as measured using EEG frequency power but also fMRI based global signal. Importantly, we found evidence that microstates and vigilance levels are causally related and the changes in vigilance cause

changes in the parameters of microstates. The observed associations had predictive power, and temporal dynamics of vigilance could be, to some extent, reconstructed based on the microstate parameters. The parameters of EEG microstates were highly associated with vigilance and global signal. In particular, we consistently found a relation between the duration of microstate C to both vigilance levels and global signal. We found as well that occurrence but not the duration of microstate class B was correlated with the vigilance level. This suggests that duration and occurrence of microstates manifest different psychophysiological mechanisms. This view gets support from recent research that suggests that psychiatric disorders only affect one of these two microstates selectively (Michel & Koenig, 2017). Importantly, to estimate the vigilance levels, we follow with the definition and algorithm described in (Falahpour et al., 2018). Compared to alternative approaches like VIGALL (Hegerl & Hensch, 2014, Olbrich et al., 2009, Strauss et al., 2015), the approach used here has the benefit that it produces continuous measures of vigilance and does not require electrooculography data.

4.1. Vigilance loss during eyes-closed resting state

In the current study vigilance was estimated as the ratio of the square root power in the alpha to the power in the delta and theta bands. Similar metrics have been used in multiple studies (Horovitz et al., 2008, Jobert et al., 1994, Larson-Prior et al., 2009, Wong et al., 2013). We validated the metrics and showed that for our sample it provides comparable results to a widely used vigilance classification algorithm VIGALL (Olbrich et al., 2009). We found a gradual decline in vigilance over the

eyes-closed resting state recordings. While occurrence of sleep epochs is thought to be a common phenomenon during typical rest conditions and we therefore cannot exclude the potential occurrence of sleep epochs (Olbrich et al., 2009, Tagliazucchi & Laufs, 2014), in our study only data from two subjects showed clear indications of sleep onset as quantified using VIGALL. One possible reason for this could be that our data were acquired in the beginning of the experimental day for both data sets which insured subjects remained highly motivated and aroused. This agrees with the reports about high variability in the time spent in the sleep across individual fMRI centers which in many cases tested in (Tagliazucchi & Laufs 2014) stayed close to zero.

4.2. Role of microstates A and B

We found negative associations between the occurrence of microstates A and B with the vigilance level. This observation goes in line with recent studies which link the presence of these two microstates to primary sensory processes. Microstate class B was suggested to be associated with the visual resting state network (Britz et al., 2010, Custo et al., 2017), a claim which was further supported by an increase in duration of the microstate class B in eyes-open rest (Seitzman et al., 2017) and was shown to be associated with visual imagery thoughts (Lehmann et al., 1998). The sources of the microstate class A seem to be in the temporal areas and can be associated with the auditory resting state network (Britz et al., 2010, Custo et al., 2017). While it does not affect our interpretation, it is noteworthy that a recent study (Milz et al., 2016), however, contrary to the studies above, reported evidence that microstate class A could be related to visual and microstate class B to verbalization processes.

4.3. Role of microstate C

The functional role of the microstate class C is still unclear (Michel & Koenig, 2017). Recent studies suggest a relation of microstate class C to cognitive control processes (Britz et al., 2010). However, the decrease of the duration of microstate class C in serial subtraction tasks (Bréchet et al., 2019, Seitzman et al., 2017) and visualization tasks (Milz et al., 2016) puts forward the hypothesis that it might reflect task-negative network activity (Michel & Koenig, 2017). Our observation of a positive association of the duration of the microstate class C with vigilance favors the role of this microstate in cognitive control processes. Also, microstate class C is characterized by frontal to occipital topography with posterior predominance of activity. Taken together with the fact that induction of the different microstates is mainly determined by strength of the power in the alpha band (Milz et al., 2017), an increased contribution of the microstate class C may reflect higher occipital alpha power. Loss of vigilance is characterized by a gradual shift of alpha power from the occipital towards frontal brain regions followed by a decrease in power in the alpha band and an increase in power in delta and theta frequency ranges that characterize drowsiness states (Olbrich et al., 2009). Thereby the highest occipital alpha power is typically associated with the most vigilant state. Thus, it is not surprising, that we observe strong positive associations of the parameters of this microstate with vigilance.

4.4. Role of microstate D

We observed a positive association between the duration of the microstate class D and the vigilance level. This could be explained by a number of recent studies suggesting that microstate class D is characterized by sources in middle and superior frontal areas as well as superior and inferior parietal areas (Britz et al., 2010, Custo et al., 2017) and has been hypothesized to be associated with the dorsal attention network. This hypothesis is further supported by the observation that occurrence and duration of this microstate increased during serial subtraction task (Bréchet et al., 2019, Seitzman et al., 2017). We note however, that,

somewhat contrary to this hypothesis, (Milz et al., 2016) reported the highest duration and occurrence of the microstate class D during rest in comparison with a number of cognitive tasks. This suggests that microstate class D might reflect focus switching and reflexive aspects of attention. While we cannot reject or confirm any of these two based on these results, we find it noteworthy that both theories indirectly implicate the relation between microstate D and the vigilance state.

4.5. EEG microstates and sleep

The parameters of EEG microstates have been previously investigated during sleep and sleep disorders. Patients with frontotemporal dementia, a disorder that is associated by frequent excessive daytime sleepiness comorbidity (McCarter et al., 2016), were shown to have reduced duration of microstate class C (Nishida et al., 2013). Reduced duration of microstate class C was also reported for insomnia patients (Wei et al., 2018). These reports agree with our observation that higher vigilance states are associated with increased duration of microstate class C. However, narcolepsy patients, that also suffer from excessive daytime sleepiness, were characterized by increased duration of microstate class C and reduced contribution of microstate class A (Drissi et al., 2016) during wakefulness and reduced duration of microstate class C during N1 and N3 sleep stages (Kuhn et al., 2015). These contradicting finding in patients suffering from similar symptoms indicate the complexity of vigilance regulation mechanisms. Interestingly, in the study that investigated differences of EEG microstate parameters during different sleep stages (Brodbeck et al., 2012), presence of N1 sleep was characterized by reduced duration and contribution of microstate class A, reduced contribution of microstate class B, increased duration and contribution of microstate class C and increased probability of transitions towards map C. These findings confirm strong association of parameters of microstate classes A, B and C with sleep. The observed opposite effects of drowsiness and sleep on them are pointing towards non-linearity of the relation between EEG microstate parameters and vigilance and should be addressed in further studies. Related, the interrelation between drowsiness, sleep and vigilance states is still understudied field, that requires further efforts to be clarified (Hasan, 1996, Oken et al., 2006).

4.6. Relation to the fMRI global signal

The fMRI global signal is known to arise from multiple effects, and resolving these effects is important for the interpretation of fMRI data. While some parts of global signal are non-neural (breathing, motion, etc.), there is also a contribution from neural activity, including fluctuation in vigilance (Falahpour et al., 2018, Wong et al., 2016, Wong et al., 2013), coordinated by regions such as basal forebrain (Turchi et al., 2018). In line with recent studies (Falahpour et al., 2018, Wong et al., 2016, Wong et al., 2013) we found a negative association between vigilance and the fMRI global signal. We additionally found that fMRI global signal was associated with the duration and contribution of microstate class C and the contribution of microstate class A. The present results support the partial neural origin of the global signal and suggest that the association between microstate parameters and global signal is mainly mediated by vigilance. However, parameters of microstate class B as well as transition probabilities between microstate classes did not show any association with the global signal. This suggests that the change in vigilance may likely affect brain dynamics on multiple levels where the mechanisms that affect microstate parameters and global signal are essentially different.

4.7. The potential mediating role of cingulate cortex

It is interesting to note that an increasing number of recent studies, using source reconstruction techniques, suggest that the cingulate cortex

is a common source for all microstate classes (Custo et al., 2017, Pascual-Marqui et al., 2014). In line with these findings, multimodal imaging EEG-fMRI studies provided evidence that attenuation of vigilance levels leads to an increase in activity of the anterior part (Olbrich et al., 2009) while caffeine intake leads to alterations of BOLD activity in the posterior part of the cingulate cortex (Falahpour et al., 2018). Taken together, considering the role of cingulate cortex and arousal, these studies suggest the activity of the cingulate cortex to mediate the causal relation between vigilance level and appearance of microstates sequences.

4.8. Prediction accuracy

We found that the observed association between parameters of the microstates and vigilance time series has predictive power. Using support vector machine regression, we could predict vigilance fluctuations with accuracy which is statistically significant but not numerically high. This suggests that vigilance levels and EEG microstate parameters are not reflecting necessary the same processes. Such view receives further support from observations that next to the power in the alpha frequency band, microstates are additionally related to delta, theta, and higher frequency bands (Khanna et al., 2015). Taken together and considering that vigilance level is a more fundamental characteristic of the organism, which is also partially modulated by the body, we speculate that the time course of microstates is influenced by vigilance through multiple systems.

4.9. Analysis of microstates in psychiatric disorders

The finding that parameters of EEG microstates have temporal dynamics which are partly modulated by vigilance state has far reaching implications when microstates are studied in the context of psychiatric disorders. Patients suffering from psychiatric disorders often show abnormal sleep behavior and/or altered temporal vigilance structure. In light of the findings presented in this paper, the potential changes found in microstates could be essentially related to changes in vigilance which might or might not be a symptom or manifestation of the neural mechanism of the disorder, but indicate a rather straightforward change in sleep behavior.

5. Conclusion

We provided evidence for correlations and, crucially, causal relations between the fluctuations of vigilance level and temporal dynamics of the EEG microstates within the first 10 minutes of rest. We found that duration and contribution of microstate class C were positively, while occurrence and contribution of microstate classes A and B were negatively associated with vigilance. Changes in vigilance caused changes in EEG microstate parameters. The observed findings highlight the importance of taking vigilance levels into consideration in EEG microstate parameter investigations. We suggest that the cingulate cortex may be a potential mediator of the observations we made and the fact that EEG microstates reacted to the changes in vigilance level potentially by integrating multiple neural mechanisms.

CRediT authorship contribution statement

Marina Krylova: Conceptualization, Methodology, Software, Validation, Formal analysis, Data curation, Writing - original draft, Writing - review & editing. **Sarah Alizadeh:** Conceptualization, Methodology, Supervision, Data curation. **Igor Izyurov:** Data curation. **Vanessa Teckentrup:** Methodology, Formal analysis, Methodology, Writing - review & editing. **Catie Chang:** Data curation, Writing - review & editing. **Johan van der Meer:** Data curation. **Michael Erb:** Data curation. **Nils Kroemer:** Methodology, Writing - review & editing. **Thomas Koenig:** Data curation. **Martin Walter:** Conceptualization, Validation, Resources, Supervision, Project administration, Data curation. **Hamidreza Jamalabadi:** Conceptualization, Methodology, Validation, Resources, Supervision, Data curation, Writing - original draft, Writing - review & editing.

Acknowledgements

Data and code availability

The data of the data set 2 and/or code used in the current study are available from the corresponding authors upon reasonable request subject to a formal data sharing agreement with Prof. Martin Walter. Data set 1 can only be shared with formal agreement with Prof. Martin Walter and Biologische Heilmittel HEEL GmbH, Germany.

Appendix A. Validation of the vigilance estimation approach

To validate reliability of a frequency power based vigilance detection approach (for details see methods section 1.3) we estimated the vigilance scores using an EEG-based vigilance classification algorithm VIGALL 2.1 (Hegerl et al., 2017) for the first dataset. The classification is based on the distribution of cortical current density activity over four distinct regions of interest (O1, O2, F3, F4). An estimate of the cortical current density is separately computed for the delta/theta and the alpha frequency range using LORETA (Pascual-Marqui et al., 2002). The individual alpha center frequency was automatically detected for each subject, and the alpha band was defined as ± 2 Hz around the individual alpha peak frequency. The delta/theta band was set between 3 and 7 Hz. Each epoch was classified into one of seven different brain states along a wake–sleep continuum (alertness: 0, A1, A2, A3; drowsiness: B1, B2/3; and sleep onset: C). To compare the time course of vigilance fluctuations between frequency based and VIGALL based approaches, we assigned a vigilance score ranging from 1 to 7 to each EEG-vigilance state (1 represents the lowest (stage C) and 7 the highest (stage 0) vigilance state).

We analyzed the association between frequency power based and conventional VIGALL vigilance estimations (see Fig. A.1). The Pearson linear correlation showed that mean vigilance levels ($r = 0.72$, $p < 10 \times -5$) and slopes of the vigilance curves ($r = 0.53$, $p = 0.001$) in the two approaches considered here were strongly correlated. To inspect the temporal similarity between two approaches, the correlation between the vigilance time-series detected by both approaches were calculated separately for each subject. One-sample t-test on the xDF-adjusted z-scored subject-level correlation coefficients showed highly significant group level effect ($t = 13.29$, $p < 10 \times -14$). Given the similarity between the vigilance estimates for the eyes-closed resting state recordings obtained from VIGALL and the frequency power-based vigilance detection approaches, authors decided to stick to the latter as absence of electrooculographic data is a serious limitation for the VIGALL estimations. Also, the frequency power-based vigilance estimate provides a continuous measure which is more suitable for correlation analysis than discrete VIGALL-based scores. Fig. A1.
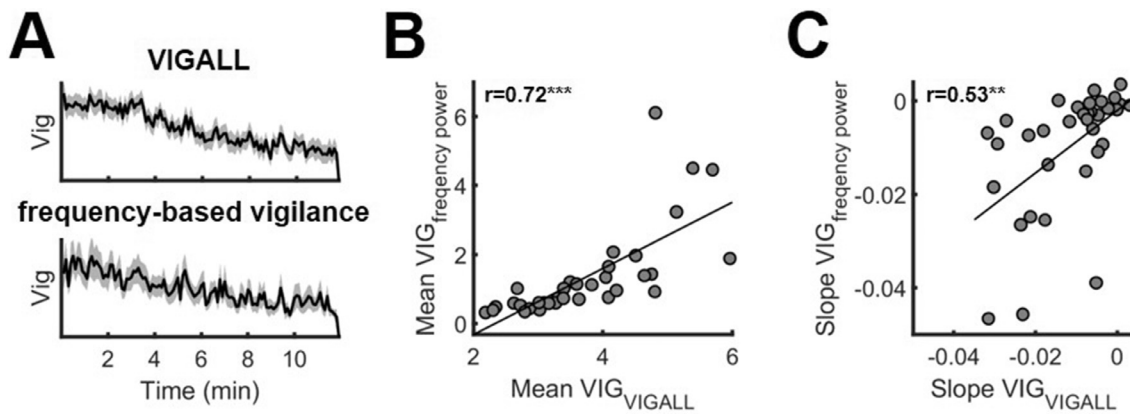
Fig. A1. Association between the frequency power based and conventional VIGALL vigilance estimations for the first dataset. A: Group average vigilance time course for the VIGALL2.1 based (on top) and frequency power based (on bottom) vigilance estimations. Shadows represent standard error of the mean across all subjects. For both vigilance estimation approaches we observe a vigilance decline that has similar slope. B: Association of the mean vigilance levels for the two ways of vigilance estimation. Each dot indicates data of one subject. C: Association of the slopes of vigilance curve for the two ways of vigilance estimation. Each dot indicates data of one subject. Stars correspond to the significance levels ($p < 0.001$ - ***, $0.001 < p < 0.01 - $**, $0.01 < p < 0.05 - $*). The vigilance scores are highly correlated between the two approaches for vigilance estimation.

Appendix B. Association of the time courses of the microstate parameters and time course of EEG frequency power

To investigate frequency dependence of the microstate parameters, we have investigated the association between the time courses of the microstate parameters and power alpha and delta+theta frequency ranges. To obtain the temporal dynamics of EEG power fluctuation, power spectral density of EEG was estimated for each channel using non-overlapping Hamming window (Data set 1: 500 points, 2.0s temporal width. Data set 2: 450 points, 1.8s temporal width). Relative power in the alpha (7-13 Hz) and delta+theta (1-7 Hz) frequency band were calculated as root mean square (rms) amplitude in the band of interest divided by the rms amplitudes in the frequency range (1-20 Hz) at each time point. The occipital alpha power was estimated as a mean power in alpha frequency band over occipital channels (O1, O2, Oz, PO7, PO8, PO3, PO4 and POz). The overall alpha power was estimated by averaging the EEG power in frequency band of interest over all channels.

Similar to the vigilance analysis, the frequency power time-series were smoothed by calculating the mean value within a non-overlapping window of 3 TR and the correlation between the time courses of the microstate parameters and frequency power fluctuations were calculated

for each subject separately. The group level effects were revealed using one-sample t-tests on the xDF-adjusted z-scored correlation coefficients. To account for multiple comparisons, results were corrected using False Discovery Rate (FRD) correction for 12 tests. For illustrative purposes, we report the results only for duration and occurrence of microstates and only for the first dataset (Table B1).

We found that the associations between microstate parameters and alpha power fluctuations are strongly similar for occipital and all channel alpha power, indicating huge contribution of the occipital alpha to the all channel alpha power estimates. We observed that the parameters of microstate class A and C were associated with power changes both in alpha and delta+theta bands. However, duration of microstate class D was positively correlated only with alpha power changes. We also found that occurrence of microstate class B was associated with vigilance time course, but not correlated with power changes in alpha or delta+theta bands separately. Taken together, these observations indicate complexity of the vigilance phenomenon. We think that in-depth investigation of the relation between EEG frequency powers and EEG microstates is a research question, that goes beyond the scope of the current manuscript and should be further addressed. Table B1.

Table B1
This table lists the results (t-values and p-values) of the one-sample t-test on the on the xDF-adjusted z-scored subject-level correlation coefficients for the correlation the time courses of the microstate parameters and vigilance, all channel alpha power, occipital alpha power and all channel delta theta power. Significant results ($p < 0.05$) after FDR correction for 12 comparisons are marked in bold. The results show that associations between microstate parameters and vigilance are not exclusively mediated by changes in a specific frequency band, indicating complexity of the vigilance phenomenon.

		A	B	C	D
Vigilance	Duration	**t = -4.65 p = 1 × 10-4**	t = -0.32 p = 0.818	**t = 5.79 p = 7 × 10-6**	**t = 3.66 p = 0.002**
	Occurrence	**t = -4.94 p = 7 × 10-5**	**t = -2.53 p = 0.028**	t = 0.80 p = 0.514	t = 0.07 p = 0.943
All channel alpha power	Duration	**t = -4.66 p = 1 × 10-4**	t = -0.65 p = 0.570	**t = 5.11 p = 8 × 10-5**	**t = 2.83 p = 0.016**
	Occurrence	**t = -4.16 p = 0.001**	t = -1.86 p = 0.096	t = 1.93 p = 0.096	t = 0.37 p = 0.717
Occipital alpha power	Duration	**t = -4.45 p = 3 × 10-4**	t = -0.51 p = 0.673	**t = 5.38 p = 3 × 10-5**	**t = 3.14 p = 0.007**
	Occurrence	**t = -4.24 p = 4 × 10-4**	t = -2.01 p = 0.071	t = 2.09 p = 0.070	t = 0.35 p = 0.728
All channel delta + theta power	Duration	**t = 5.03 p = 1 × 10-4**	t = -0.30 p = 0.835	**t = -4.86 p = 1 × 10-4**	t = -1.92 p = 0.127
	Occurrence	**t = 3.50 p = 0.003**	t = 1.50 p = 0.240	t = -1.44 p = 0.213	t = 0.07 p = 0.944

Appendix C. Association of the mean vigilance level and mean values of the microstate parameters

Table C1

This table lists the results (r-values and p-values) of all preformed correlations between the mean vigilance level and mean values of the microstate parameters. Significant results (p < 0.05) after FDR correction for 12 comparisons are marked in bold. Mean duration and contribution of the microstate class C are positively associated with vigilance level while occurrence of the microstates class B shows a robust trend toward significant negative association with vigilance level in both investigated data sets.

		A	B	C	D
Data set 1	Duration	r = -0.12 p = 0.645	r = -0.03 p = 0.866	**r = 0.62 p = 7 × 10-4**	**r = 0.43 p = 0.033**
	Occurrence	**r = -0.59 p = 0.001**	**r = -0.43 p = 0.033**	r = 0.19 p = 0.411	r = -0.11 p = 0.645
	Contribution	**r = -0.40 p = 0.037**	r = -0.34 p = 0.084	**r = 0.65 p = 4 × 10-4**	r = 0.06 p = 0.798
Data set 2	Duration	r = -0.16 p = 0.613	r = -0.21 p = 0.514	**r = 0.73 p = 0.005**	r = 0.38 p = 0.169
	Occurrence	r = -0.46 p = 0.131	r = -0.55 p = 0.058	r = 0.41 p = 0.161	r = -0.12 p = 0.675
	Contribution	r = -0.38 p = 0.169	r = -0.45 p = 0.131	**r = 0.63 p = 0.022**	r = 0.07 p = 0.776

Table C2

This table lists the results (r-values and p-values) of all preformed correlations between the mean vigilance level and mean values of the transition probability for transitions between four microstate classes. Significant results (p < 0.05) after FDR correction for 12 comparisons are marked in bold. For both data sets mean transition probabilities from microstate A towards microstate class C are positively, while transition probabilities from microstate class D towards microstate class A are negatively associated with vigilance levels.

	Data set 1	Data set 2
A → B	r = -0.26 p = 0.214	r = -0.20 p = 0.549
A → C	**r = 0.66 p = 3 × 10-4**	**r = 0.59 p = 0.050**
A → D	r = -0.26 p = 0.214	r = -0.33 p = 0.293
B → A	r = -0.20 p = 0.350	r = -0.36 p = 0.275
B → C	r = 0.30 p = 0.179	r = 0.46 p = 0.140
B → D	r = 0.08 p = 0.643	r = 0.22 p = 0.549
C → A	r = -0.32 p = 0.164	r = -0.15 p = 0.640
C → B	r = -0.37 p = 0.090	r = -0.35 p = 0.275
C → D	r = 0.13 p = 0.490	r = -0.06 p = 0.818
D → A	r = -0.41 p = 0.064	**r = -0.62 p = 0.050**
D → B	r = -0.18 p = 0.297	r = 0.07 p = 0.818
D → C	**r = 0.48 p = 0.023**	r = 0.46 p = 0.140

Appendix D. Association of the vigilance time course and the time courses of the microstate parameters

Table D1

This table lists the results (t-values and p-values) of the one-sample t-test on the xDF-adjusted z-scored subject-level correlation coefficients for the correlation the vigilance time-series and the time courses of the microstate parameters. Significant results (p < 0.05) after FDR correction for 12 comparisons are marked in bold. Time courses of the duration and contribution of the microstate class C as well as duration of the microstate class D are positively, while time courses of the occurrence and contribution of the microstates classes A and B are negatively associated with changes of vigilance level in both investigated data sets.

		A	B	C	D
Data set 1	Duration	**t = -4.65 p = 1 × 10-4**	t = -0.32 p = 0.818	**t = 5.79 p = 7 × 10-6**	**t = 3.66 p = 0.002**
	Occurrence	**t = -4.94 p = 7 × 10-5**	**t = -2.53 p = 0.028**	t = 0.80 p = 0.514	t = 0.07 p = 0.943
	Contribution	**t = -5.96 p = 7 × 10-6**	**t = -2.29 p = 0.038**	**t = 5.92 p = 7 × 10-6**	**t = 2.39 p = 0.034**
Data set 2	Duration	t = 0.11 p = 0.986	t = -0.35 p = 0.877	**t = 4.68 p = 0.001**	**t = 2.67 p = 0.026**
	Occurrence	**t = -5.00 p = 0.001**	**t = -3.60 p = 0.006**	t = -0.02 p = 0.986	t = -0.86 p = 0.537
	Contribution	**t = -3.94 p = 0.004**	**t = -3.15 p = 0.011**	**t = 3.21 p = 0.011**	t = 1.57 p = 0.200

Table D2

This table lists the results (t-values and p-values) of the one-sample t-test on the on the xDF-adjusted z-scored subject-level correlation coefficients for the correlation the vigilance time-series and the time courses of the transition probabilities for transitions between four microstate classes. Significant results (p < 0.05) after FDR correction for 12 comparisons are marked in bold. Time courses of the transition probabilities for transitions from microstate class A towards microstate class C are positively associated with vigilance time-series.

	Data set 1	Data set 2
A → B	t = -1.96 p = 0.117	t = -1.79 p = 0.216
A → C	**t = 6.46 p = 3 × 10-6**	t = 3.07 p = 0.064
A → D	t = -1.33 p = 0.209	t = -0.50 p = 0.872
B → A	t = -2.02 p = 0.117	t = -0.97 p = 0.690
B → C	t = 0.67 p = 0.505	t = 0.16 p = 0.958
B → D	t = 1.69 p = 0.137	t = 1.95 p = 0.201
C → A	**t = -3.24 p = 0.011**	t = -0.01 p = 0.991
C → B	t = -1.66 p = 0.137	t = -2.85 p = 0.064
C → D	t = 1.63 p = 0.137	t = 0.76 p = 0.788
D → A	**t = -4.05 p = 0.002**	t = -2.14 p = 0.185
D → B	t = 1.62 p = 0.137	t = 0.35 p = 0.873
D → C	**t = 2.56 p = 0.046**	t = 0.46 p = 0.872

Appendix E. Association of the global signal time-series and the time courses of the microstate parameters

Table E1

This table lists the results (t-values and p-values) of the one-sample t-test on the xDF-adjusted z-scored subject-level correlation coefficients for the correlation the global signal time-series and the time courses of the microstate parameters. Significant results (p < 0.05) after FDR correction for 12 comparisons are marked in bold. Time courses of the duration and contribution of the microstate class C are negatively, while time course of the contribution of the microstate class A is positively associated with GS time-series in both investigated data sets.

		A	B	C	D
Data set 1	Duration	**t = 2.68 p = 0.035**	t = 1.20 p = 0.301	**t = -3.47 p = 0.014**	t = -1.07 p = 0.317
	Occurrence	t = 2.22 p = 0.081	t = 0.13 p = 0.895	t = -1.52 p = 0.239	t = -1.54 p = 0.239
	Contribution	**t = 2.90 p = 0.027**	t = 1.17 p = 0.301	**t = -3.31 p = 0.014**	t = -1.31 p = 0.299
Data set 2	Duration	t = 1.59 p = 0.261	t = -0.30 p = 0.771	**t = -3.01 p = 0.046**	t = -0.34 p = 0.771
	Occurrence	t = 1.61 p = 0.261	t = 1.16 p = 0.392	t = -1.58 p = 0.261	t = 1.31 p = 0.355
	Contribution	**t = 2.81 p = 0.046**	t = 1.08 p = 0.392	**t = -2.83 p = 0.046**	t = 0.63 p = 0.647

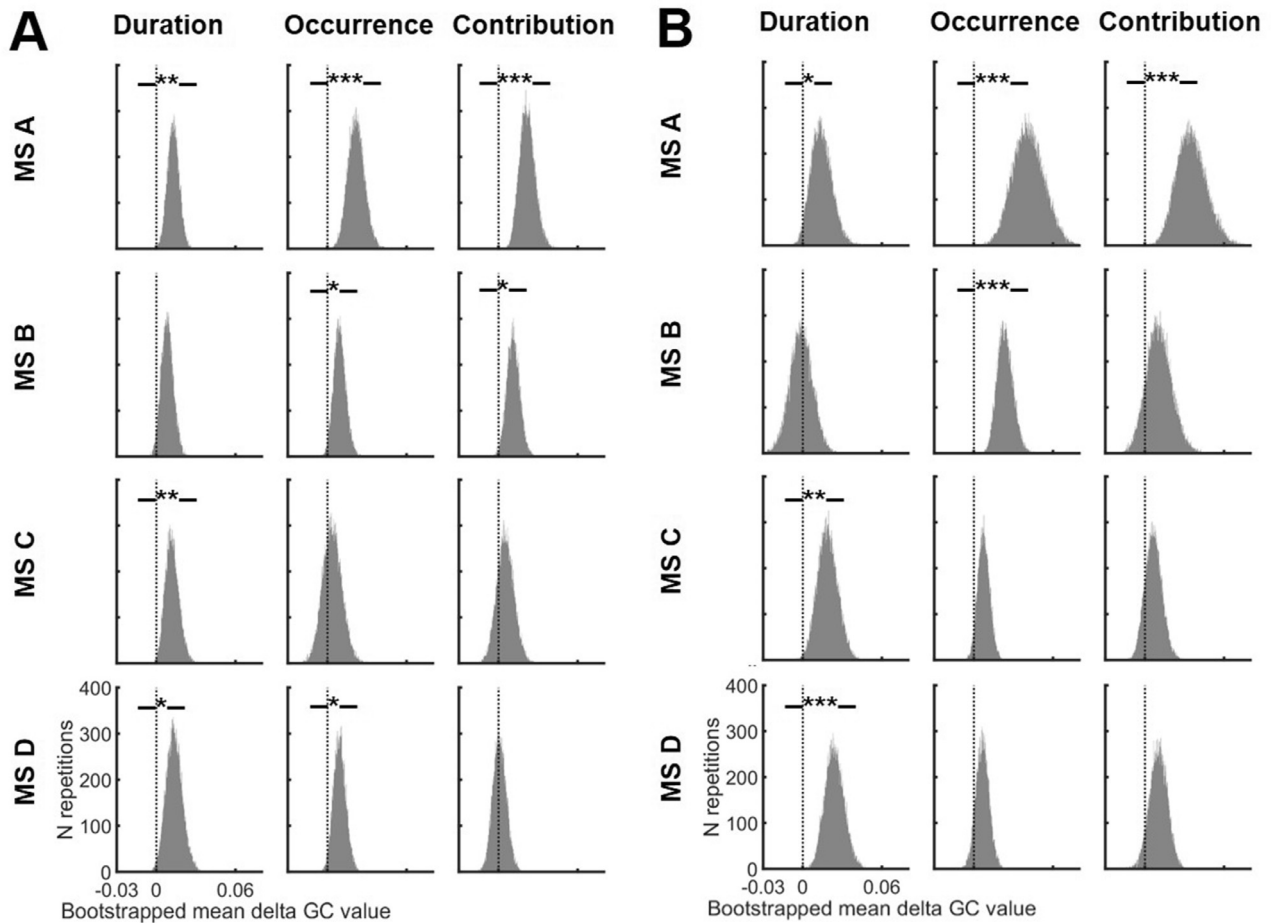## Appendix F. Causal effects of vigilance on microstate parameters

Fig. F1

Fig. F1. Granger causality estimates suggest that vigilance fluctuations Granger-cause changes in EEG microstate parameters. Depicted are bootstrapped distributions (50000 repetitions) of mean delta GC values (VIG → MS) - (MS → VIG). For both datasets, the mean delta GC significantly different from zero for duration, occurrence and contribution of microstate class A, occurrence of microstate class B and duration of microstate classes C and D, indicating overall causal effect of changes in vigilance levels on the changes of the parameters of microstates.

References

Afyouni, S., Smith, S.M., Nichols, T.E., 2019. Effective degrees of freedom of the Pearson's correlation coefficient under autocorrelation. NeuroImage 199, 609–625.

Allefeld, C., Graben, P.B., Kurths, J., 2008. Advanced Methods of Electrophysiological Signal Analysis and Symbol Grounding?: Dynamical Systems Approaches to Language. Nova Publishers.

Allen, P.J., Josephs, O., Turner, R., 2000. A method for removing imaging artifact from continuous EEG recorded during functional MRI. Neuroimage 12, 230–239.

Barnett, L., Seth, A.K., 2014. The MVGC multivariate Granger causality toolbox: a new approach to Granger-causal inference. J. Neurosci. Method 223, 50–68.

Bréchet, L., Brunet, D., Birot, G., Gruetter, R., Michel, C.M., Jorge, J., 2019. Capturing the spatiotemporal dynamics of self-generated, task-initiated thoughts with EEG and fMRI. NeuroImage.

Britz, J., Van De Ville, D., Michel, C.M., 2010. BOLD correlates of EEG topography reveal rapid resting-state network dynamics. NeuroImage 52, 1162–1170.

Brodbeck, V., Kuhn, A., von Wegner, F., Morzelewski, A., Tagliazucchi, E., et al., 2012. EEG microstates of wakefulness and NREM sleep. Neuroimage 62, 2129–2139.

Cori, J.M., Anderson, C., Soleimanloo, S.S., Jackson, M.L., Howard, M.E., 2019. Narrative review: Do spontaneous eye blink parameters provide a useful assessment of state drowsiness. Sleep Med. Rev..

Custo, A., Van De Ville, D., Wells, W.M., Tomescu, M.I., Brunet, D., Michel, C.M., 2017. Electroencephalographic resting-state networks: source localization of microstates. Brain Connect. 7, 671–682.

De Gennaro, L., Vecchio, F., Ferrara, M., Curcio, G., Rossini, P.M., Babiloni, C., 2005. Antero-posterior functional coupling at sleep onset: changes as a function of increased sleep pressure. Brain Res. Bull. 65, 133–140.

Delorme, A., Makeig, S., 2004. EEGLAB: an open source toolbox for analysis of single-trial EEG dynamics including independent component analysis. J. Neurosci. Method 134, 9–21.

Dimitriadis, S., Laskaris, N., Micheloyannis, S., 2015. Transition dynamics of EEG-based network microstates during mental arithmetic and resting wakefulness reflects task-related modulations and developmental changes. Cognit. Neurodyn. 9, 371–387.

Drissi, N.M., Szakács, A., Witt, S.T., Wretman, A., Ulander, M., et al., 2016. Altered brain microstate dynamics in adolescents with narcolepsy. Front. Hum. Neurosci. 10, 369.

Faber, P.L., Lehmann, D., Barendregt, H., Kaelin, M., Gianotti, L.R., 2005. Increased duration of EEG microstates during meditation. Brain Topogr. 18, 131.

Falahpour, M., Chang, C., Wong, C.W., Liu, T.T., 2018. Template-based prediction of vigilance fluctuations in resting-state fMRI. NeuroImage 174, 317–327.

Fallgatter, A., Brandeis, D., Strik, W., 1997. A robust assessment of the NoGo-anteriorisation of P300 microstates in a cued Continuous Performance Test. Brain Topogr. 9, 295–302.

Fallgatter, A.J., Bartsch, A.J., Strik, W.K., Mueller, T.J., Eisenack, S.S., et al., 2001. Test-retest reliability of electrophysiological parameters related to cognitive motor control. Clin. Neurophysiol. 112, 198–204.

Hallez, H., Vanrumste, B., Grech, R., Muscat, J., De Clercq, W., et al., 2007. Review on solving the forward problem in EEG source analysis. J. Neuroeng. Rehab. 4, 46.

Hasan, J., 1996. Past and future of computer-assisted sleep analysis and drowsiness assessment. J. Clin. Neurophysiol. 13, 295–313.

Hegerl, U., Hensch, T., 2014. The vigilance regulation model of affective disorders and ADHD. Neurosci. Biobehav. Rev. 44, 45–57.

Hegerl U., Sander C., Ulke C., Böttger D., Hensch T., et al. 2017. Vigilance Algorithm Leipzig (VIGALL) Version 2.1 Manual.

Horovitz, S.G., Fukunaga, M., de Zwart, J.A., van Gelderen, P., Fulton, S.C., et al., 2008.

Low frequency BOLD fluctuations during resting wakefulness and light sleep: A simultaneous EEG-fMRI study. Hum. Brain Mapp. 29, 671–682.

Jobert, M., Schulz, H., Jähnig, P., Tismer, C., Bes, F., Escola, H., 1994. A computerized method for detecting episodes of wakefulness during sleep based on the alpha slow-wave index (ASI). Sleep 17, 37–46.

Katayama, H., Gianotti, L.R., Isotani, T., Faber, P.L., Sasada, K., et al., 2007. Classes of multichannel EEG microstates in light and deep hypnotic conditions. Brain Topogr. 20, 7–14.

Khanna, A., Pascual-Leone, A., Farzan, F., 2014. Reliability of resting-state microstate features in electroencephalography. PLoS One 9, e114163.

Khanna, A., Pascual-Leone, A., Michel, C.M., Farzan, F., 2015. Microstates in resting-state EEG: current status and future directions. Neurosci. Biobehav. Rev. 49, 105–113.

Kikuchi, M., Koenig, T., Munesue, T., Hanaoka, A., Strik, W., et al., 2011. EEG microstate analysis in drug-naive patients with panic disorder. Plos One 6, e22912.

Kindler, J., Hubl, D., Strik, W.K., Dierks, T., Koenig, T., 2011. Resting-state EEG in schizophrenia: auditory verbal hallucinations are related to shortening of specific microstates. Clin. Neurophysiol. 122, 1179–1182.

Koenig, T., Lehmann, D., Merlo, M.C., Kochi, K., Hell, D., Koukkou, M., 1999. A deviant EEG brain microstate in acute, neuroleptic-naive schizophrenics at rest. Eur. Arch. Psychiatry Clin. Neurosci. 249, 205–211.

Koenig, T., Prichep, L., Lehmann, D., Sosa, P.V., Braeker, E., et al., 2002. Millisecond by millisecond, year by year: normative EEG microstates and developmental stages. Neuroimage 16, 41–48.

Koenig, T., Studer, D., Hubl, D., Melie, L., Strik, W.K., 2005. Brain connectivity at different time-scales measured with EEG. Philos. Trans. R. Soc. B 360, 1015–1023.

Kuhn, A., Brodbeck, V., Tagliazucchi, E., Morzelewski, A., von Wegner, F., Laufs, H., 2015. Narcoleptic patients show fragmented EEG-microstructure during early NREM sleep. Brain Topogr. 28, 619–635.

Larson-Prior, L.J., Zempel, J.M., Nolan, T.S., Prior, F.W., Snyder, A.Z., Raichle, M.E., 2009. Cortical network functional connectivity in the descent to sleep. Proc. Natl. Acad. Sci. 106, 4489–4494.

Lehmann, D., Faber, P.L., Galderisi, S., Herrmann, W.M., Kinoshita, T., et al., 2005. EEG microstate duration and syntax in acute, medication-naive, first-episode schizophrenia: a multi-center study. Psychiatry Res. Neuroimaging 138, 141–156.

Lehmann, D., Ozaki, H., Pal, I., 1987. EEG alpha map series: brain micro-states by space-oriented adaptive segmentation. Electroencephalogr. Clin. Neurophysiol. 67, 271–288.

Lehmann, D., Pascual-Marqui, R.D., Strik, W.K., Koenig, T., 2010. Core networks for visual-concrete and abstract thought content: a brain electric microstate analysis. Neuroimage 49, 1073–1079.

Lehmann, D., Skrandies, W., 1984. Spatial analysis of evoked potentials in man–a review. Progr. Neurobiol. 23, 227–250.

Lehmann, D., Strik, W., Henggeler, B., König, T., Koukkou, M., 1998. Brain electric microstates and momentary conscious mind states as building blocks of spontaneous thinking: I. Visual imagery and abstract thoughts. Int. J. Psychophysiol. 29, 1–11.

Mathis, J., Hess, C.W., 2009. Sleepiness and vigilance tests. Swiss Med. Wkly. 139, 214–219.

McCarter, S.J., Louis, E.K.S., Boeve, B.F., 2016. Sleep disturbances in frontotemporal dementia. Curr. Neurol. Neurosci. Rep. 16, 85.

Michel, C.M., Koenig, T., 2017. EEG microstates as a tool for studying the temporal dynamics of whole-brain neuronal networks: A review. NeuroImage.

Milz, P., Faber, P.L., Lehmann, D., Koenig, T., Kochi, K., Pascual-Marqui, R.D., 2016. The functional significance of EEG microstates–Associations with modalities of thinking. NeuroImage 125, 643–656.

Milz, P., Pascual-Marqui, R.D., Achermann, P., Kochi, K., Faber, P.L., 2017. The EEG microstate topography is predominantly determined by intracortical sources in the alpha band. Neuroimage 162, 353–361.

Moosmann, M., Schönfelder, V.H., Specht, K., Scheeringa, R., Nordby, H., Hugdahl, K., 2009. Realignment parameter-informed artefact correction for simultaneous EEG–fMRI recordings. Neuroimage 45, 1144–1150.

Nishida, K., Morishima, Y., Yoshimura, M., Isotani, T., Irisawa, S., et al., 2013. EEG microstates associated with salience and frontoparietal networks in frontotemporal dementia, schizophrenia and Alzheimer's disease. Clin. Neurophysiol. 124, 1106–1114.

Oken, B.S., Salinsky, M.C., Elsas, S., 2006. Vigilance, alertness, or sustained attention: physiological basis and measurement. Clin. Neurophysiol. 117, 1885–1901.

Olbrich, S., Mulert, C., Karch, S., Trenner, M., Leicht, G., et al., 2009. EEG-vigilance and BOLD effect during simultaneous EEG/fMRI measurement. Neuroimage 45, 319–332.

Olbrich, S., Sander, C., Minkwitz, J., Chittka, T., Mergl, R., et al., 2012. EEG vigilance regulation patterns and their discriminative power to separate patients with major depression from healthy controls. Neuropsychobiology 65, 188–194.

Pascual-Marqui, R.D., Esslen, M., Kochi, K., Lehmann, D., 2002. Functional imaging with low-resolution brain electromagnetic tomography (LORETA): a review. Methods Findings Exp Clin. Pharmacol. 24, 91–95.

Pascual-Marqui R.D., Lehmann D., Faber P., Milz P., Kochi K., et al. 2014. The resting microstate networks (RMN): cortical distributions, dynamics, and frequency specific information flow. arXiv preprint arXiv:1411.1949.

Randerath, W., Verbraecken, J., Andreas, S., Arzt, M., Bloch, K.E., et al., 2017. Definition, discrimination, diagnosis and treatment of central breathing disturbances during sleep. Eur. Respir. J. 49.

Schiller, B., Koenig, T., Heinrichs, M., 2019. Oxytocin modulates the temporal dynamics of resting EEG networks. Sci. Rep. 9, 1–9.

Seitzman, B.A., Abell, M., Bartley, S.C., Erickson, M.A., Bolbecker, A.R., Hetrick, W.P., 2017. Cognitive manipulation of brain electric microstates. Neuroimage 146, 533–543.

Strauss, M., Paucke, M., Sander, C., Hegerl, U., 2015. Vigilance regulation in adult ADHD. Pharmacopsychiatry 25, A98.

Strijkstra, A.M., Beersma, D.G., Drayer, B., Halbesma, N., Daan, S., 2003. Subjective sleepiness correlates negatively with global alpha (8–12 Hz) and positively with central frontal theta (4–8 Hz) frequencies in the human resting awake electroencephalogram. Neurosci. Lett. 340, 17–20.

Tagliazucchi, E., Laufs, H., 2014. Decoding wakefulness levels from typical fMRI resting-state data reveals reliable drifts between wakefulness and sleep. Neuron 82, 695–708.

Turchi, J., Chang, C., Frank, Q.Y., Russ, B.E., David, K.Y., et al., 2018. The basal forebrain regulates global resting-state fMRI fluctuations. Neuron 97, 940–952 e4.

van der Meer, J.N., Pampel, A., Van Someren, E.J.W., Ramautar, J.R., van der Werf, Y.D., et al., 2016. Carbon-wire loop based artifact correction outperforms post-processing EEG/fMRI corrections-A validation of a real-time simultaneous EEG/fMRI correction method. NeuroImage 125, 880–894.

Wei, Y., Ramautar, J.R., Colombo, M.A., Te Lindert, B.H., Van Someren, E.J., 2018. EEG microstates indicate heightened somatic awareness in insomnia: Toward objective assessment of subjective mental content. Front. Psychiatry 9, 395.

Wong, C.W., DeYoung, P.N., Liu, T.T., 2016. Differences in the resting-state fMRI global signal amplitude between the eyes open and eyes closed states are related to changes in EEG vigilance. NeuroImage 124, 24–31.

Wong, C.W., Olafsson, V., Tal, O., Liu, T.T., 2013. The amplitude of the resting-state fMRI global signal is related to EEG vigilance measures. NeuroImage 83, 983–990.

Zanesco, A.P., King, B.G., Skwara, A.C., Saron, C.D., 2020. Within and between-person correlates of the temporal dynamics of resting EEG microstates. NeuroImage, 116631.